Strain rate and temperature dependence of Omori law scaling constants of AE data: Implications for earthquake foreshock-aftershock sequences

Ira O. Ojala,[1] Ian G. Main,[2] and Bryne T. Ngwenya[2]

Received 18 June 2004; revised 14 November 2004; accepted 1 December 2004; published 29 December 2004.

[1] Little is known about the temperature and strain rate dependence of acoustic emission AE activity (AE). Hence, we carried out a preliminary series of flow-through triaxial compression tests on porous sandstones at different temperatures and strain rates. The AE data exhibits clear foreshock and aftershock sequences with respect to the dynamic failure of the test specimen. Significant AE activity starts less than 5 min before sample failure irrespective of the strain rate. The increase in the AE event rate is steeper and the foreshock exponent p' is smaller in the slow strain rate tests. It could be the reason why there are no easily recognisable foreshock sequences for most individual earthquakes. The aftershock decay parameter p is a linear function of test temperature as it has also been inferred for natural seismicity. The seismic b-value decreases systematically with increasing deformation rate suggesting a greater proportion of small cracks in the slow strain rate tests. Hence, the AE activity is a function of both strain rate and temperature. *INDEX TERMS:* 5102 Physical Properties of Rocks: Acoustic properties; 5104 Physical Properties of Rocks: Fracture and flow; 5134 Physical Properties of Rocks: Thermal properties. **Citation:** Ojala, I. O., I. G. Main, and B. T. Ngwenya (2004), Strain rate and temperature dependence of Omori law scaling constants of AE data: Implications for earthquake foreshock-aftershock sequences, *Geophys. Res. Lett.*, *31*, L24617, doi:10.1029/2004GL020781.

1. Introduction

[2] Acoustic emission (AE) due to microcrack growth precedes the macroscopic failure of a rock sample under constant stress [*Lockner and Byerlee*, 1977; *Yanagidani et al.*, 1985] or constant strain rate loading [*Mogi*, 1962; *Scholz*, 1968]. It is perhaps due to the similarity in their statistical behaviour that acoustic emissions can be considered analogous to earthquake foreshock-aftershock sequences. The temporal [*Hirata*, 1987], spatial [*Hirata et al.*, 1987] and size distribution [*Mogi*, 1962] of AE events follows a power law, just as it is commonly observed for earthquakes [*Frohlich and Davis*, 1993; *Utsu et al.*, 1995]. Such power-law scaling can be considered indicative of self-similarity in the AE and earthquake source process [*Hirata*, 1987].

[3] Both AE and earthquake data follow the modified Omori law for the earthquake and laboratory aftershock rate R_a that is given by

$$R_a \propto (c_a + t - t_m)^{-p} \tag{1}$$

where c_a is a constant and t_m is the time of the main shock [*Utsu et al.*, 1995; *Main*, 2000]. Similarly, foreshock sequences can be characterised using

$$R_f \propto (c_f + t_m - t)^{-p'} \tag{2}$$

where c_f is a constant, p' is the exponent for foreshocks and R_f is the foreshock rate. The estimated p-values for earthquake aftershock sequences range from 0.6 to 2.5 with a median of 1.1 [*Utsu et al.*, 1995]. For AE activity the exponent p ranges from 0.8 to 2.3 [*Hirata*, 1987].

[4] The time evolution of AE and earthquake data also display considerable differences. Laboratory rock fracture is dominated by a large number of foreshocks while seismicity in the Earth's crust is characterised by an abundance of aftershocks [*Main*, 2000]. Laboratory studies have also reported a more gradual acceleration of seismic event rate than the few recorded foreshock sequences for earthquakes [*Mogi*, 1967; *Liakopoulou-Morris et al.*, 1984; *Helmstetter et al.*, 2003]. Our experimental data confirm that the acceleration of AE activity becomes more rapid as strain rate decreases. Since crustal strain rates are considerably slower than laboratory rates, these data provide an explanation for the lack of easily recognisable foreshock sequences for earthquakes. In addition, the Omori law decay parameter p (1) is directly proportional to temperature in our tests. A similar temperature dependence is displayed by crustal earthquakes [*Utsu et al.*, 1995].

2. Methodology

[5] Two Permian Aeolian sandstones were used for the tests. Clashach sandstone is well sorted, quartz cemented, subarcosic arenite with medium to coarse grains (250–500 μm). It is composed of 89% quartz and 11% feldspar. Locharbriggs sandstone has a grain size of 100 μm. It is composed of 83% quartz, 16% feldspar, 1% hematite and weakly cemented with hematite and illite coatings on grain surfaces.

[6] The test methodology is the same as in *Ojala et al.* [2003, 2004]. The samples were deformed in a triaxial ($\sigma_1 > \sigma_2 = \sigma_3$) testing apparatus. The water flow in and out of the sample was 0.2 ml/min. The confining pressure was fixed at 13.5 MPa within the brittle regime. The back-pressure

[1]GeoForschungsZentrum Potsdam, Telegrafenberg, Potsdam, Germany.
[2]School of GeoSciences, University of Edinburgh, Edinburgh, UK.

0094-8276/04/2004GL020781

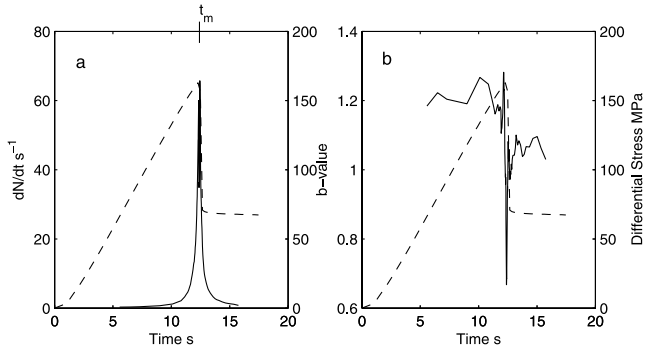

Figure 1. The temporal evolution of differential stress (dashed) and (a) AE event rate (b) the seismic b-value 80°C Clashach test at $2.7*10^{-5}$ s^{-1}.

equalled the atmospheric pressure at 0.1 MPa. The jacketed sample was heated to the appropriate temperature and loaded to hydrostatic conditions. Highly reactive fine particles were removed by flushing with distilled water for 24 hours at a constant flow rate of 0.2 ml/min. Tests were carried out at temperatures of 25–80°C at different loading rates. The strain rates ranged from 10^{-5} to 10^{-8} s^{-1} during the linear elastic deformation phase.

[7] The AE technique was used for remotely monitoring microcrack growth inside the rock sample. A single Panametrics 125 kHz piezoelectric transducer measured the AE activity. The signals were amplified by 40 dB using a Panametrics pre-amplifier and recorded using MISTRAS AE system. The amplitude threshold for the AE signals was set at 50 dB. A higher amplitude threshold was chosen in order to ensure adequate disk space for data storage.

3. Results

[8] The stress-strain curves for this test series have been published in *Ojala et al.* [2003, 2004]. In this communication we attend to the effect of temperature and strain rate on the recorded AE activity. Figure 1 illustrates the temporal evolution of the differential stress, AE event rate *dN/dt* and the seismic b-value for a 80°C Clashach test at $2.7*10^{-5}$ s^{-1}. The b-values (Table 1) were calculated using the maximum likelihood method of *Aki* [1965] from an incremental frequency distribution of the measured AE amplitudes. No distinct strain hardening phase was observed at such a high strain rate although significant AE activity began prior to the peak stress. After the peak stress was attained *dN/dt* decreased dramatically to a period of apparent quiescence, which can be attributed to critical crack coalescence [*Main and Meredith*, 1991] or over-saturation of the measuring equipment [*Liakopoulou-Morris et al.*, 1994]. Dynamic instability marked the specimen failure at t_m(1). It was followed by a quick recovery in AE event rate and a subsequent decrease in a manner similar to earthquake aftershocks. The similarity in the temporal evolution of the AE foreshock and aftershock sequences with respect to specimen failure time was a characteristic feature of the Clashach tests. The Locharbriggs sandstone exhibited a more gradual acceleration of the AE event rate, followed by a period of apparent quiescence and less pronounced aftershock activity.

[9] Table 1 lists the event rate statistics for all of the tests. There is no correlation between the total number of recorded AE events N_t with lithology, strain rate or test temperature due to the different flaw distributions inside the test specimen at the start of each test. The highest AE event rates of over 100 events/min occur only few minutes prior to sample failure irrespective of the strain rate, as shown in Table 2. The majority of the recorded AE events occurred after the peak stress had been attained. The proportion of AE events that occurred after peak stress increased systematically with decreasing strain rate. These AE data are in good agreement with the more pronounced strain softening phase in the slow strain rate tests [*Ojala et al.*, 2004].

[10] The time evolution of the AE event rate exhibited a clear dependence on the applied loading rate, as illustrated in Figure 2. The acceleration of the AE activity became systematically more rapid as the strain rate decreased.

[11] The b-value decreased with increasing stress. A b-value minimum b_f was observed immediately prior to

Table 1. Mechanical and AE Data for the Flow-Through Tests on Clashach (C) and Locharbriggs (L) Sandstones (S)[a]

S	$\dot{\varepsilon}$ s^{-1}	T °C	σ_{max} MPa	N_p	N_f	N_t	A_{max} dB	b_t	b_f
L	2.5×10^{-7}	25	81.3	1186	4495	5035	81	1.21	1.06
L	2.8×10^{-7}	40	77.8	564	2788	3573	79	1.26	1.06
L	3.3×10^{-7}	40	82.3	595	3371	3452	97	1.23	0.96
L	3.1×10^{-7}	60	81.4	713	1789	1922	97	1.24	1.07
L	3.0×10^{-5}	80	81.2	1620	3257	3495	97	1.09	0.74
L	3.2×10^{-6}	80	80.8	191	948	987	96	1.13	0.99
L	3.4×10^{-7}	80	79.9	604	6541	6687	79	1.21	1.06
L	2.8×10^{-8}	80	77.7	177	922	1467	68	1.24	1.10
C	2.5×10^{-7}	25	166.7	997	6185	8196	98	0.96	0.74
C	2.2×10^{-7}	40	140.4	852	2094	2496	97	1.04	0.68
C	2.7×10^{-7}	60	162.8	277	4200	5201	98	1.02	0.60
C	2.7×10^{-5}	80	162.8	997	1870	2495	98	1.03	0.67
C	3.2×10^{-6}	80	169.3	1294	1374	1603	97	1.01	0.81
C	3.3×10^{-7}	80	134.6	518	5881	9881	95	1.08	0.70
C	3.3×10^{-8}	80	122.6	105	947	1616	97	1.09	0.87

[a]The b-values were calculated in 200-event windows with a running step of 25 events in order to determine the b-value minimum that preceded specimen failure b_f. b_t is the seismic b-value for a whole test. N_p, N_f and N_t are the number of AE events up to the peak stress, to specimen failure and for the entire test, respectively.

Table 2. Omori Law Fits to the AE Event Rate dN/dt on Clashach (C) and Locharbriggs (L) Sandstones (S)[a]

S	$\dot{\varepsilon}$ s^{-1}	T °C	c_f min	p′	k_1	r^2	c_a min	p	k_2	r^2	t_a min
L	2.5×10^{-7}	25	0.17	0.84	6.12	0.87	0.01	1.05	4.24	0.96	2
L	2.8×10^{-7}	40	0.19	0.93	6.07	0.92	0.01	1.13	3.74	0.97	2
L	3.3×10^{-7}	40	2.43	0.82	9.04	0.93	0.34	1.09	7.86	0.96	1
L	3.1×10^{-7}	60	0.01	0.76	4.70	0.91	0.01	1.18	3.32	0.98	1
L	3.0×10^{-5}	80	4.37	6.81	18.4	0.95	0.14	1.97	4.89	0.96	2
L	3.2×10^{-6}	80	0.33	1.63	5.80	0.93	0.01	1.30	2.95	0.99	2
L	3.4×10^{-7}	80	0.11	0.80	6.42	0.88	0.02	1.37	3.22	0.97	4
L	2.8×10^{-8}	80	0.01	0.88	4.53	0.97	0.01	1.29	3.12	0.98	1
C	2.5×10^{-7}	25	4.27	2.14	10.8	0.89	0.01	0.79	5.05	0.95	12
C	2.2×10^{-7}	40	0.05	1.02	5.92	0.92	0.05	1.29	4.86	0.99	1
C	2.7×10^{-7}	60	0.01	0.83	6.23	0.91	0.02	1.20	5.69	0.93	10
C	2.7×10^{-5}	80	0.56	2.71	7.04	0.94	0.11	1.26	5.60	0.96	1
C	3.2×10^{-6}	80	0.42	1.96	6.28	0.96	0.01	0.96	4.47	0.92	2
C	3.3×10^{-7}	80	1.58	1.98	9.18	0.95	0.08	1.23	5.76	0.95	5
C	3.3×10^{-8}	80	0.06	1.31	4.86	0.98	0.04	1.28	4.66	0.98	1

[a]The foreshock R_f and aftershock R_a rates scale as $R_f = e^{k_1}(c_f + t_m - t)^{-p'}$ and $R_a = e^{k_2}(c_a + t - t_m)^{-p}$, respectively. t_a measures the time before main shock t_m during which the AE rate exceeds 100 min^{-1}.

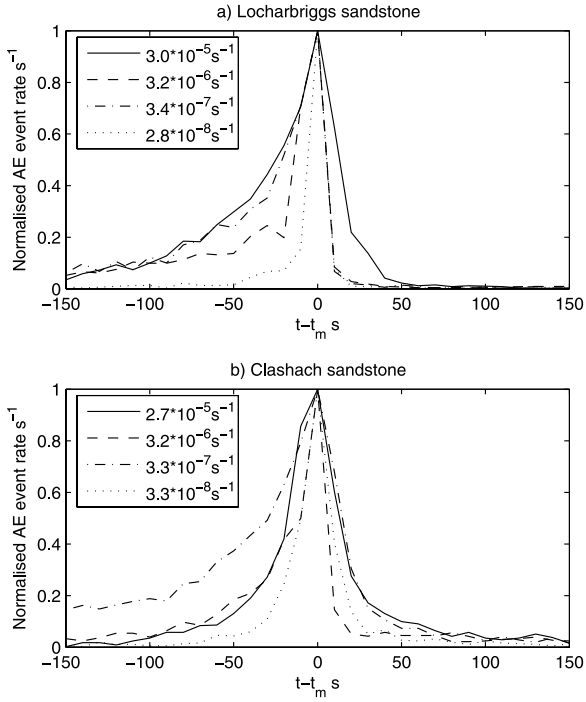

Figure 2. The evolution of the normalised AE event rate for the four 80°C (a) Locharbriggs and (b) Clashach tests from 10^{-5} to 10^{-8} s^{-1}. The AE activity displayed a strain rate dependence, indicating that specimen failure time t_m becomes more difficult to predict as the strain rate decreases.

dynamic failure of the test specimen for both sandstones. The minima b_f ranged from 0.60 to 0.87 and 0.96 to 1.10 for the Clashach and Locharbriggs sandstones. The calculated b-values ranged from 0.60 to around 1.26.

[12] The b-values b_f and b_t increased with decreasing strain rate. For the Locharbriggs sandstone, the maximum observed event amplitude A_{max} decreased with decreasing strain rate while b_t was a linear function of the logarithm of the strain rate, given by

$$b_t = 0.85 - 0.053 \log \dot{\varepsilon} \tag{3}$$

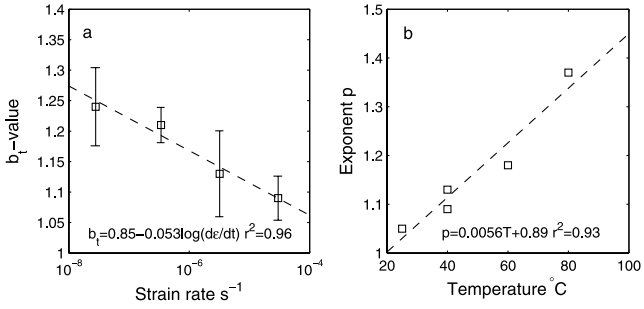

Figure 3. (a) The calculated b_t-values for the Locharbriggs sandstone tests as function of strain rate for the 80°C tests. The error bars indicate the nominal 95% confidence limit $1.96b(n)^{-1/2}$ where n is the number of events used for the b-value calculation [*Aki*, 1965]. (b) The aftershock decay parameter p as a function of temperature for the Locharbriggs 10^{-7} s^{-1} tests.

with an r-squared value of 0.96, as illustrated in Figure 3. These observations suggest that there were a greater number of smaller events in the slow strain rate tests than in the high strain rate tests. Some of the smaller magnitude events could be caused by stress corrosion fracturing, since this is likely to be the dominant crack growth mechanism at slow strain rates [*Ojala et al.*, 2003].

[13] The AE sequences were fitted to the Omori formulae (1–2). The AE event rate (dN/dt) was calculated for every ten consecutive events. The best fit to the Omori law was obtained by allowing c_a and c_f to take different values for each test, given by c_f and c_a, respectively. The optimal Omori law fits to the AE data are listed in Table 2. The goodness of fit to the Omori formulae was best for the very slow strain rate (10^{-8} s^{-1}) AE data (Figure 4). The Locharbriggs aftershock decay parameter p was a function of temperature, given by

$$p = 0.0056T + 0.89 \tag{4}$$

with an r-squared value of 0.93, as illustrated in Figure 3. This observation is consistent with the higher p-values that have been obtained for earthquake data in areas with high heat flow [*Utsu et al.*, 1995].

4. Discussion

[14] The time evolution and size distribution of the recorded AE activity display a clear strain rate dependence. This is not surprising since the mechanical and hydraulic properties of these sandstones also depend on the strain rate [*Ojala et al.*, 2003, 2004]. However, it is an important observation because crustal strain rates (10^{-14} to 10^{-16} s^{-1}) are considerably smaller than laboratory ones. It is questionable whether the results of high strain rate (10^{-5} or 10^{-6} s^{-1}) laboratory tests can be applied directly to crustal

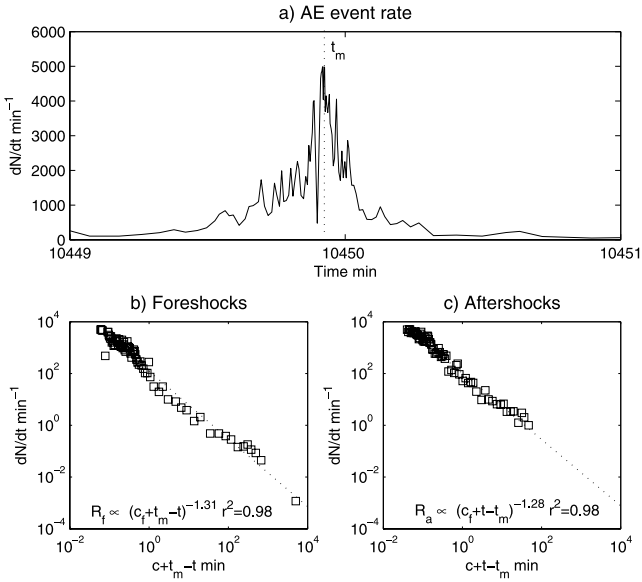

Figure 4. The (a) AE event rate, (b) foreshock sequence and (c) aftershock sequence for a 80°C Clashach test that was carried out at a strain rate of 3.3×10^{-8} s^{-1}. Maximum dN/dt coincides with specimen failure at t_m.

processes. More research should be carried out into the kinetic effect of a chemically active environment on the brittle deformation properties of rocks. All time and rate dependence of rock mechanical properties is ultimately caused by such physico-chemical processes [*Costin*, 1987; *Ojala et al.*, 2003].

[15] The AE event rate exhibits fore- and aftershock sequences associated with the dynamic failure of the tests specimen. Although aftershock sequences are not commonly recorded in laboratory tests, the temporal evolution of the AE event rate is very similar to the observations of *Meredith et al.* [1990] for Darley Dale sandstone. The AE event rate obeys the Omori formulae (1–2) with high correlation coefficients. The majority of the Omori law exponents are close to unity, as it is observed for earthquakes [*Utsu et al.*, 1995] and laboratory rock fracture [*Hirata*, 1987]. The exponent p' for foreshocks decreases with decreasing strain rate for both sandstones. This observation is not predicted by the stochastic model of *Mogi* [1962], which assumes that the fracture probability μ_m is a an exponential function of the stress rate and time. Instead, our data suggest that the prediction of rock failure becomes increasingly difficult as the strain rate decreases, as indicated by the steeper increase in the AE event rate. Since crustal strain rates are considerably smaller than laboratory rates such strain rate dependence explain the lack of easily recognisable foreshocks preceding earthquakes. Furthermore, the Locharbriggs exponents p for aftershocks are consistently higher than the exponent p' for foreshocks. The higher p-values might be related to the fractured state of the rock specimen [*Mogi*, 1967].

[16] Sample failure is preceded by a decrease in the seismic b-value followed by a recovery after faulting. A single b-value minimum is observed immediately before dynamic instability, in the fault nucleation stage. Similar precursory changes in b-value have been reported for earthquakes [*Von Seggern*, 1980], volcanic events [*Vinciguerra*, 1999] and for laboratory rock fracture [*Meredith et al.*, 1990]. The b-values for the different tests cluster around one, in accordance with the observed b-values for earthquakes [*Frohlich and Davis*, 1993]. The Locharbriggs amplitudes decrease and b-values increase systematically with decreasing strain rate. These observations agree with *Sano et al.* [1982] who reported an increase in b-value associated with decreasing dilatant strain rate in their uniaxial tests on Oshima granite. Similarly, *Yabe* [2002] observed a b-value decrease associated with increased sliding velocity on his shear tests on Westerly granite. Hence, the size distribution of AE events display a strain rate dependence for both intact and faulted specimen. It is possible that the same underlying mechanism generates both of these phenomena. Natural faults may heal and strengthen between earthquakes and resemble the intact rock samples that were used in this study [*Lockner*, 1993]. Moreover, the slip on faults is likely to involve the breaking of local asperities due to the roughness of fault surfaces [*Lockner and Byerlee*, 1993].

[17] The aftershock decay parameter p correlates with test temperature. This formula (4) is remarkably similar to the regression $p = 0.692 + 0.000994T$ obtained for earthquake aftershocks in the Tohoku district of Japan [*Utsu et al.*, 1995]. In our tests the dependence of p on test temperature is more pronounced, since $p \propto 0.0056T$. It has been suggested that the positive correlation with surface heat flow and exponent p stems from a faster rate of stress relaxation in higher temperature areas [*Mogi*, 1967; *Utsu et al.*, 1995].

5. Conclusions

[18] Clear fore- and aftershock sequences that are well modelled by the Omori law accompany sample failure in our tests. The foreshock exponent p' decreases and the b-value increases with decreasing strain rate. The aftershock exponent p increases with test temperature. The observations show that AE activity depends on the strain rate and temperature.

[19] **Acknowledgments.** Thanks to Stephen Elphick, Alexander Hart and Denis McLaughlin for technical support and associate editor A. Zollo and two anonymous reviewers for a through review. The work was funded by Edinburgh University Faculty of Science, The Finnish Cultural Foundation and the Väisälä Foundation.

References

Aki, K. (1965), Maximum likelihood estimate of b in the formula $\log N = a - bm$ and its confidence limits, *Bull. Earthquake Res. Inst. Univ. Tokyo*, *43*, 237–239.

Costin, L. S. (1987), Time-dependent deformation and failure, in *Fracture Mechanics of Rock*, edited by B. K. Atkinson, pp. 167–215, Elsevier, New York.

Frohlich, C., and S. D. Davis (1993), Teleseismic b values; or, much Ado about 1.0, *J. Geophys. Res.*, *98*, 631–644.

Helmstetter, A., P. Sornette, and J. R. Grasso (2003), Mainshocks are aftershocks of conditional foreshocks: How do foreshock statistical properties emerge from aftershock laws?, *J. Geophys. Res.*, *108*(B1), 2046, doi:10.1029/2002JB001991.

Hirata, T. (1987), Omori's power law aftershock sequences of microfracturing in rock fracture experiment, *J. Geophys. Res.*, *92*, 6215–6221.

Hirata, T., T. Satoh, and K. Ito (1987), Fractal structure of spatial distribution of microfracturing in rock, *Geophys. J. R. Astron. Soc.*, *90*, 369–374.

Liakopoulou-Morris, F., I. G. Main, B. R. Crawford, and B. G. D. Smart (1994), Microseismic properties of a homogeneous sandstone during fault nucleation and frictional sliding, *Geophys. J. Int.*, *119*, 219–230.

Lockner, D. A. (1993), The role of acoustic emission in the study of rock fracture, *Int. J. Rock Mech. Min. Sci. Geomech. Abstr.*, *30*, 883–899.

Lockner, D., and J. Byerlee (1977), Acoustic emission and creep in rock at high confining pressure and differential stress, *Bull. Seismol. Soc. Am.*, *67*, 247–258.

Lockner, D. A., and J. D. Byerlee (1993), How geometrical constraints contribute to the weakness of mature faults, *Nature*, *363*, 250–252.

Main, I. (2000), A damage mechanics model for power law creep and earthquake aftershock and foreshock sequences, *Geophys. J. Int.*, *142*, 151–161.

Main, I. G., and P. G. Meredith (1991), Stress corrosion constitutive laws as a possible mechanism for intermediate-term and short-term seismic quiescence, *Geophys. J. Int.*, *107*, 363–372.

Meredith, P. G., I. G. Main, and C. Jones (1990), Temporal variations in seismicity during quasi-static and dynamic rock failure, *Tectonophysics*, *175*, 249–268.

Mogi, K. (1962), Study of elastic shocks caused by the fracture of heterogeneous materials and its relation to earthquake phenomena, *Bull. Earthquake Res. Inst. Univ. Tokyo*, *40*, 125–173.

Mogi, K. (1967), Earthquakes and fractures, *Tectonophysics*, *5*, 35–55.

Ojala, I. O., B. T. Ngwenya, I. G. Main, and S. C. Elphick (2003), Correlation of microseismic and chemical properties of brittle deformation in Locharbriggs sandstone, *J. Geophys. Res.*, *108*(B5), 2268, doi:10.1029/2002JB002277.

Ojala, I. O., B. T. Ngwenya, and I. G. Main (2004), Loading rate dependence of permeability evolution in porous aeolian sandstones, *J. Geophys. Res.*, *109*, B01204, doi:10.1029/2002JB002347.

Sano, O., M. Terada, and S. Ehara (1982), A study of the time-dependent microfracturing and strength of Oshima granite, *Tectonophysics*, *84*, 343–362.

Scholz, C. H. (1968), Microfracturing and the inelastic deformation of rock in compression, *J. Geophys. Res.*, *73*, 1417–1432.

Utsu, T., Y. Ogata, and R. S. Matsu'ura (1995), The centenary of the Omori formula for a decay law of aftershock activity, *J. Phys. Earth*, *43*, 1–33.

Vinciguerra, S. (1999), Seismic scaling exponent as a tool in detecting stress corrosion crack growth in the September–October 1989 flank eruption in Mt. Etna volcano, *Geophys. Res. Lett.*, *26*, 3685–3688.

Von Seggern, D. (1980), A random stress model for seismicity statistics and earthquake prediction, *Geophys. Res. Lett.*, *7*, 637–640.

Yabe, Y. (2002), Rate dependence of AE activity during frictional sliding, *Geophys. Res. Lett.*, *29*(10), 1388, doi:10.1029/2001GL014369.

Yanagidani, T., S. Ehara, O. Nishizawa, K. Kusunose, and M. Terada (1985), Localization of dilatancy in Ohshima granite under constant uniaxial stress, *J. Geophys. Res.*, *90*, 6840–6858.

I. O. Ojala, GeoForschungsZentrum Potsdam, Section 3.2, Telegrafenberg, D-14473 Potsdam, Germany. (ojala@gfz-potsdam.de)

I. G. Main and B. T. Ngwenya, School of GeoSciences, West Mains Road, University of Edinburgh, Edinburgh EH9 3JW, UK.